Supplement of Atmos. Meas. Tech., 19, 2329–2342, 2026
https://doi.org/10.5194/amt-19-2329-2026-supplement

Atmospheric Measurement Techniques
Open Access
EGU

Supplement of

Laminar gas inlet – Part 2: Wind tunnel chemical transmission measurement and modelling

Da Yang et al.

Correspondence to: Da Yang (da.yang@colorado.edu) and Rainer Volkamer (rainer.volkamer@colorado.edu)

Uncertainty analysis is crucial for experimental data. It quantifies the confidence in the results, identifies potential sources of error, and ensures the reliability and reproducibility of the findings. Here, we summarize our uncertainty analysis and the propagation method for these errors. We used the standard uncertainty to describe the experimental errors in the repeated measurements (e) as:

$$\boldsymbol{e = \frac{s}{\sqrt{n}}}$$

where s is the standard deviation and n is the number of data points.

To propagate the error for a linear relationship, we follow

$$\boldsymbol{e_{(x_1 \pm x_2)} = \sqrt{e_{x_1}^2 + e_{x2}^2}}$$

where x_1, x_2 represents two different variables, e_{x_1}, e_{x_2} represents the standard uncertainty from each variable.

To propagate the error for a non-linear relationship of $\frac{x_1}{x_2}$, percent relative uncertainty is used.

$$\boldsymbol{\%e = \frac{e}{mean} \times 100}$$

where $\boldsymbol{\%e}$ represents the percent relative uncertainty which is calculated by using standard uncertainty divided the mean value times 100. The propagation of error follows

$$\boldsymbol{\%e_{(\frac{x_1}{x_2})} = \sqrt{\%e_{x_1}^2 + \%e_{x2}^2}}$$

Additionally, converting the percent relative uncertainty to uncertainty for displaying the error bar as

$$\boldsymbol{e_{\frac{x_1}{x_2}} = \frac{\%e_{(\frac{x_1}{x_2})}}{100} \times mean(\frac{x_1}{x_2})}$$

During the four-day measurement period, the specific humidity in the air changed over time. As shown in Figure S1a, the specific humidity (q) has a large variation at different measurement periods. $H_2SO_4\ NCPS$ measurement results were obtained by calculating the differences between raw data in signal mode and background mode. The repeated measurement results are shown in Figure S1b. We calculate standard uncertainty to describe our error and propagate our uncertainty for $H_2SO_4\ NCPS$. The $H_2SO_4\ NCPS$ of these repeated measurements has significant variation, with a ~40% difference, at different measurement periods (Fig. S1b left y-axis). By Normalizing the $H_2SO_4\ NCPS$ using the factor of specific humidity (f_q), the difference among three repeated measurements is largely reduced to a ~15% difference (Fig. S1b right y-axis).

The sample flow features in the effective illuminated area are correlated with freestream flow velocity and size of restrictor. As shown in Figure S2a, the inlet reduces the freestream velocity to a much lower level inside the inner shroud, and a direct correlation can be seen between the freestream flow velocity (U_∞) and the sample flow velocity at the effective light area (U_{light}). Meanwhile at the same area, the radius of the sample flow shows the opposite correlation with the freestream velocity. In addition, the smaller size of restrictor results in a lower sample flow velocity (U_{light}) and a larger sample flow radius at the effective light area. A further investigation of the sample flow radius at the effective light area, as shown in Figure S2b , reveals a direct correlation between the radius of sample flow and the ratio of flow velocity at the sampling tube entrance ($U_{entrance}$) over the light area (U_{light}). Reducing the velocity ratio, $U_{entrance}/U_{light}$, can enlarge the radius of sample flow passing through the effective light area and result in generating more OH radical source.

When the sample flow is entering the sampling tube, the flow velocity slows further and results in an increase of turbulent intensity. Using our previous CFD simulation results (Yang et al., 2024), as shown in Figure S3, all simulation cases from both restrictors (12.5mm & 17mm) show that the enhancement of sample flow turbulent intensity directly inside the sampling tube, i.e., the ratio of the turbulent intensity inside the sampling tube entrance ($TI_{15}°$) to the incoming flow turbulent intensity (T_A), decreases as the ratio between flow velocity at sampling tube entrance and the incoming flow velocity ($U_{entrance}/U_A$) increases. Consist with our previous study (Yang et al., 2024) we concluded that reaching the isokinetic sampling condition can reduce the enhancement of turbulent intensity from incoming flow into the sample flow right inside the sampling tube entrance (Fig. S3).

We observed that the gas-phase $H_2SO_4\ NCPS/f_q$ measurement results still exhibited some dependence on the operating conditions of the wind tunnel, i.e., a lower normalized signal was observed when the free stream flow velocity is higher. This trend is consistently observed under different experimental configurations and operating conditions, which indicates a clear correlation between sample flow features and experimental results. To further investigate the factors at play, we studied the internal flow features of the aircraft inlet CFD simulation results. Figure S4a shows the reverse path lines from the sampling tube, and illustrates how the sample flow that travels through the UV source illuminated area enters the sampling tube.

Changing the freestream flow velocity, or the size of the restrictor, results in a different residence time inside the illuminated area (effective light area). Specifically, it results in altering the size of the region of the incoming sample flow (Fig. S2a). Moreover, the area of the sample flow, represented by its radius, that intersects with the UV illuminated area is also highly related to the velocity ratio between the average flow velocity in the effective light area and the flow velocity at the entrance of sampling tube (Fig. S2b). The higher this velocity ratio, the larger the area of the sample flow, resulting in more hydroxyl radicals entering the sampling tube. When this velocity ratio is close to 1, i.e., near isokinetic sampling conditions are achieved at the entrance of sampling tube, the sample flow has the same radius as the radius of sampling tube entrance.

To examine the correlations of normalized results ($H_2SO_4\ NCPS/f_q$) with flow features, we compared all the experimental data of the type 0 sampling line at 8 SLPM sampling flow rate with different free stream conditions. A clear correlation between the effective illuminated volume of sample flow and the measurement results ($H_2SO_4\ NCPS/f_q$) is shown in Fig. S4b. Thus, when the upstream flow velocity is high, the sample flow volume reduces and less water molecules in the sample flow can interact with the UV source. Meanwhile, the sample flow also passes quicker through the effective illuminated area, resulting in a shorter residence time and thus less hydroxyl radicals are generated. The combination of both reasons leads to lower measured signals at high freestream flow velocity such as $180 m\ s^{-1}$ for both sizes of restrictor. Moreover, as smaller size of restrictor causes a lower incoming flow velocity right outside the sampling tube, the experimental results ($H_2SO_4\ NCPS$) from two restrictors shows a separate trend (left y-axis blue in Fig. S4b). To bridge the gap between the two restrictors, we calculated the residence time of sample flow inside the effective light area from the CFD simulation results to derive the resident time factor (f_{RT}). The f_{RT} is calculated as the ratio of the resident time inside the illuminated area divided by the residence time of isokinetic sampling. The further normalized measurement results ($H_2SO_4\ NCPS \times f_{RT}/f_q$) eliminates the dependence of the signal as a function of the restrictor size. Using the above normalization, the different sampling system configurations are compared under different operating conditions in Fig. S4b.

As in the Figure S5, the normalized measurement results ($H_2SO_4\ NCPS/f_q$) from 30 $m\ s^{-1}$ freestream velocity were used to directly compare the measurement signals among different types of sampling tubes. Note that there were no measurements conducted for type 1 tube under 16 LPM conditions.

Since the sample flow in the aircraft inlet section is mainly impacted by the upstream flow conditions and laminar diffusivity can change significantly with changes of altitude, the species loss can be affected by both sampling flow rate and the laminar mass diffusivity. The gas sampling efficiency of the aircraft inlet from both altitudes and different laminar diffusivities can be approximately merged into one trend by using the flow rate divided by the laminar diffusivity as a new variable (Fig. S6).

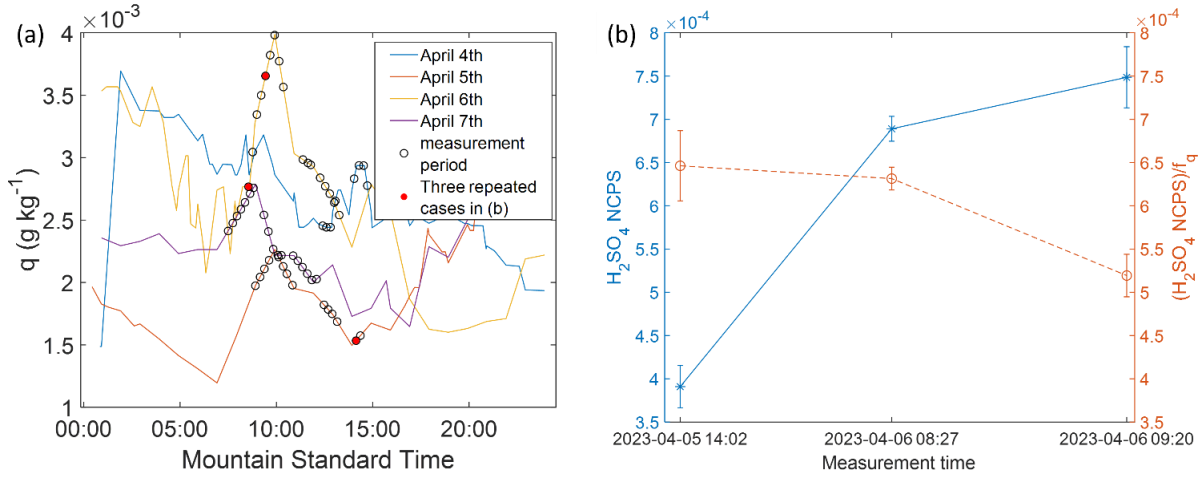

Figure S1. (a) The results of specific humidity (q) at different periods. The circles mark the average time of each period. The red circles mark the three repeated measurement periods in (b). (b) The results of H_2SO_4 NCPS compared to the H_2SO_4 NCPS results normalized by the factor of specific humidity (f_q). Three different measurement periods in (b) are operated at 30 $m\ s^{-1}$ freestream velocity with 12.5mm restrictor, 4 SLPM sampling flow rate and type 1 transmission line. The error bar is data uncertainty which follows section 2.4.

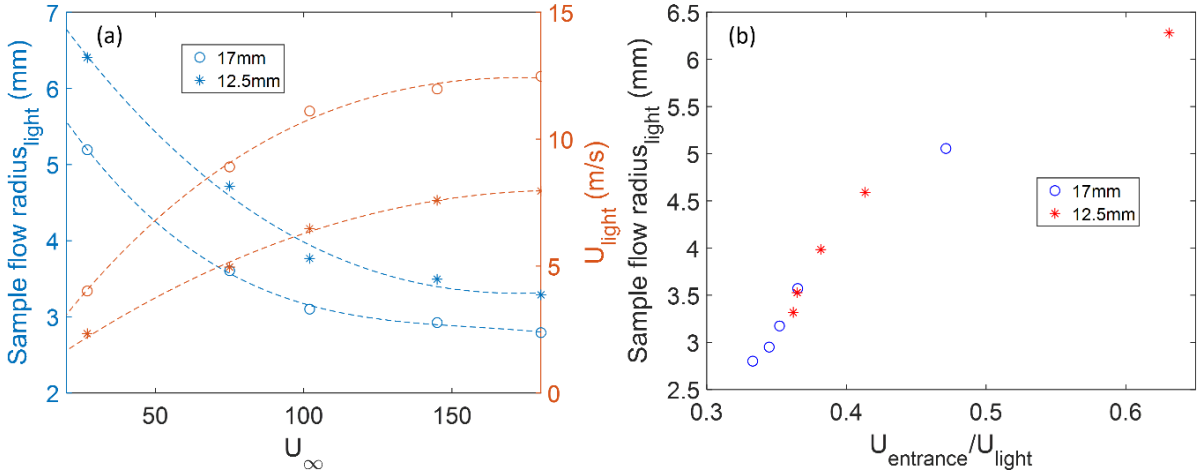

Figure S2. The simulation results of sampling flow features at effective illumination area under same sampling flow velocity 2.4 $m\ s^{-1}$. (a) The correlation between freestream velocity U_∞ and flow features at effective light area. The left y axis shows the average radius of sample flow passing the light area; the right y axis shows the average sample flow velocity U_{light} in the same area. (b) The relationship between the sample flow radius at effective illuminated area and the entrance velocity ratio, i.e., the flow velocity at the entrance of sampling tube $U_{entrance}$ divided by the flow velocity at the light area U_{light}.

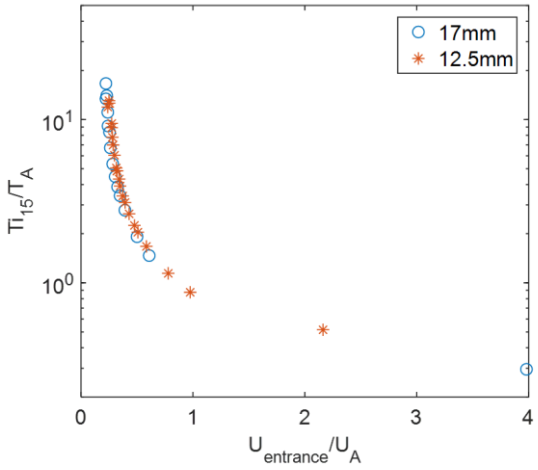

Figure S3. Correlation between the turbulent intensity enhancement directly inside the sampling tube entrance and flow velocity ratio among all inlet simulation cases from previous study. The turbulent intensity enhancement is calculated using the turbulent intensity inside the sampling tube entrance T_{15° divide the incoming flow turbulent intensity T_A. The flow ratio is calculated using the flow velocity at the entrance of the sampling tube $U_{entrance}$ divided by the incoming flow velocity U_A. All subscripts described the reference locations in previous paper (Yang et al., 2024).

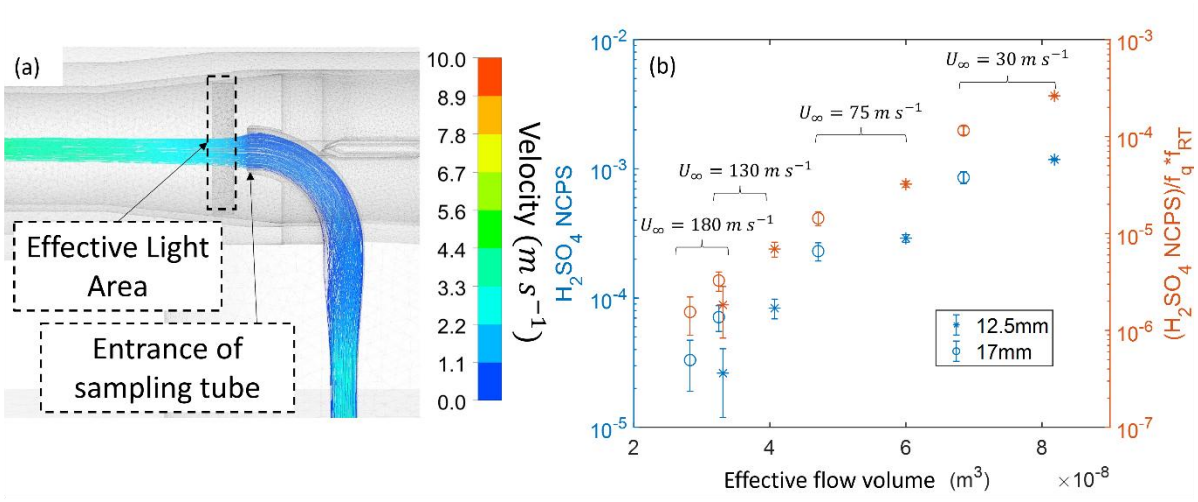

Figure S4. Factors contribute to the quantity of measurement results. (a) The reverse flow path lines from CFD simulation at freestream flow velocity 30 $m\ s^{-1}$, 12.5mm restrictor size, and 2.4 $m\ s^{-1}$sampling flow rate. The path lines are colored by the flow velocity. (b) The relationship between the measurement results of gas-phase H_2SO_4 with effective sample flow volume pass through light area. The left y axis is H_2SO_4 $NCPS$, the right y axis is the results from left y axis normalized with f_q and multiply by the f_{RT} of sample flow passing the light area. The error bar is data uncertainty which follows the description in chapter 2.4.

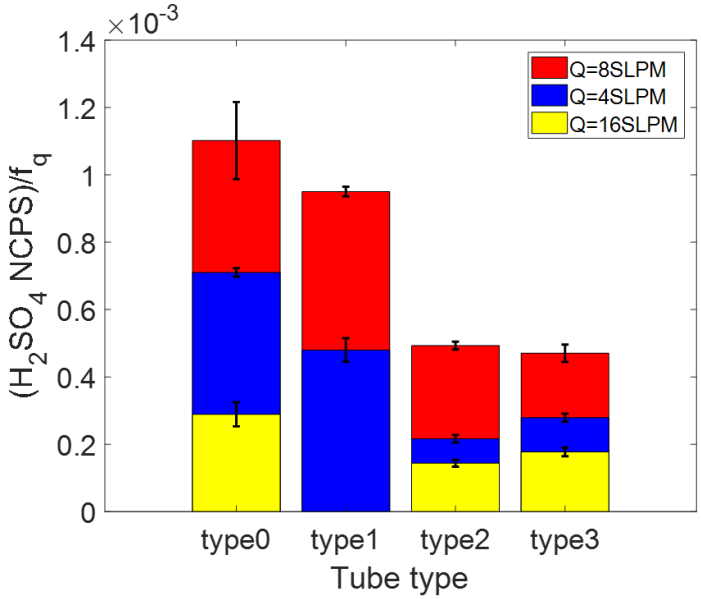

Figure S5. Comparison of different types of sampling tubes and the gas transmission efficiency: The normalized signal ($H_2SO_4\ NCPS/f_q$) through different types of sampling tubes are compared at a freestream velocity of 30 $m\ s^{-1}$, 17mm size of restrictor, for different sampling flow rates.

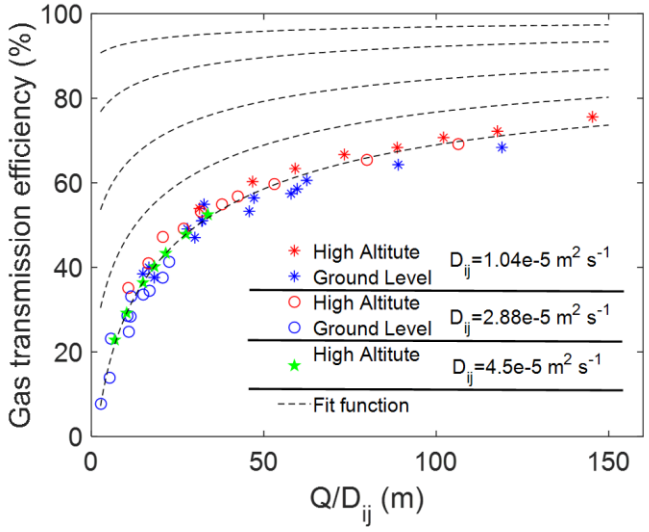

Figure S6. The unified correlation of gas sampling efficiency for both water vapor and gas-phase H_2SO_4 in the aircraft inlet section. The x axis has the volume flow rate in ($m^3\ s^{-1}$). divided by laminar diffusivity ($m^2\ s^{-1}$). The star marker presents laminar diffusivity of $1.04x10^{-5}\ m^2/s$. The circle marker presents laminar diffusivity of $2.88x10^{-5}\ m^2/s$. The green pentagram marker presents laminar diffusivity of $4.5x10^{-5}\ m^2/s$. The blue presents the ground level condition (970 mbar ambient pressure), the red and green presents the high-altitude condition (150 mbar ambient pressure). The dashed line is the fit function with different selections of sticking coefficients (α_i). The bottom dash line starts with $\alpha = 1$, followed by α values of 0.75, 0.5, 0.25, and 0.1 for each successive dashed line upward, respectively.